FULL LENGTH PAPER

COMPUTATIONAL INVESTIGATION OF EFFECT OF CASING WALL MOTION ON FLOW AND LOSSES IN AN ANNULAR TURBINE ROTOR IMPULSE CASCADE

K. Goutham Kumar
Previously M.S. Research Scholar
Thermal Turbomachines Laboratory
Department of Mechanical Engineering
Indian Institute of Technology Madras
Chennai-600 036, India

N. Sitaram
Former Professor
Thermal Turbomachines Laboratory
Department of Mechanical Engineering
Indian Institute of Technology Madras
Chennai-600 036, India
Email : nsitaram.iitm@gmail.com

Abstract

The present paper presents computational results of effect of casing wall motion on three dimensional flow and losses in an annular turbine rotor impulse cascade. The flow at the inlet of the rotor cascade is radially non uniform, which is simulated by means of an upstream nozzle blade row. Commercial CFD software is used for the computations. No slip condition is used for the case of stationary casing, whereas relative wall condition is used for the case of rotating casing. Streamlines, velocity vectors, contours of static pressure on blade tip, contours of total loss coefficient at blade exit, spanwise variation of lift coefficient, circumferentially averaged flow angles and total pressure loss coefficient and axial variation of mass averaged total pressure loss coefficient are presented for both cases. There are minor differences in the spanwise variation of various parameters for both cases. The casing wall motion reduces the losses in the region near to casing but increases in the region far away from the casing. The blade loading and lift coefficient are increased with increase in casing wall motion near the casing and reduced away from the casing. The casing motion causes a slight reduction of losses associated directly with the leakage vortex. However total losses remain nearly same.

Keywords*: Annular cascade; Turbine rotor impulse cascade; Non-uniform inlet flow; Computational investigation; Tip clearance; Losses*

Nomenclature

a = Axial chord (m)
C = Absolute velocity (m/s)
Ch = Chord (m)
Cp = Static pressure coefficient = $\frac{2\,(p_{1m} - p\,)}{\rho\,\overline{C}_{1m}^{2}}$
C_L = Lift coefficient
H = Span (m)
i = Incidence angle (deg)
p = Static pressure (Pa)
p_o = Total pressure (Pa)
Re = Reynolds number
r = Radius (m)
s = Pitch (m)
X = Non-dimensional axial distance from the blace leading edge = x/a (X=0 corresponds to LE and X=1 corresponds to TE)
x = Axial distance from the leading edge of rotor (m)
U = Blade tip speed (m/s)
α = Flow angle (from axial direction) (deg)
β = Blade angle (from axial direction) (deg)
η = Non-dimensional span = $(r\text{-}r_h) / (r_c\text{-}r_h)$; η_h=0 and η_c=1
θ = Blade camber angle (deg)
ρ = Density (kg/m^3)
τ = Tip clearance/chord x 100 (%)

Paper Code : V69 N1/930-2017. Manuscript received on 24 Nov 2015. Reviewed, revised and accepted as a Full Length Contributed Paper on 05 Dec 2016

γ = Stagger angle (from axial direction (deg)

ψ_{loss} = Total pressure loss coefficient = $\dfrac{2\,(p_{0\,1} - p_{0\,2})}{\rho\,\bar{\bar{C}}_{1m}^{2}}$

Subscripts

1 = Inlet to the rotor
2 = Exit of the rotor
c = Casing
h = Hub
m = Midspan
ref = Reference pressure
r = Radial component
u = Circumferential component
x = Axial component

Superscripts

- = Circumferentially averaged value
= = Mass averaged value

Abbreviations

CFD = Computational Fluid Dynamics
LE = Leading Edge
PS = Pressure Surface
SS = Suction Surface
TE = Trailing Edge

Introduction

Flow in axial turbines is extremely complex, three-dimensional and unsteady. It is mainly due to generation of secondary flows, tip clearance flows, hub corner-stall and blade profile wakes. Secondary and tip clearance losses form a major part of internal losses. Majority of the work in these areas has been performed by omitting relative motion between the blade and outer casing and non-uniformity in the velocity at inlet of annular cascades. In actual turbine, there is a relative motion between the blade and outer casing. The relative motion exists when there is a tip clearance between the rotating rotor blade and the stationary casing. Also the inlet velocity to the rotor is radially non-uniform. In a reference frame that is moving with turbine blade, the outer casing can be seen to move over the tip of the blade from suction side to pressure side. Tallman and Lakshminarayana [1, 2] studied the effect of casing wall motion in linear cascades. Yaras and Sjolander [3] and Yaras et al. [4] carried out experimental studies on the effect of casing motion in an axial turbine rotor linear cascade. Studies with annular cascades are limited. Available literature on numerical investigation in annular cascades mostly confined to uniform flow at inlet. For example Sell et al. [5] studied the tip clearance effects in an annular turbine cascade with uniform flow at inlet. But in actual turbine the pressure at inlet is non-uniform due to radial pressure gradient acting from hub to casing.

Objectives of the Present Investigation

The objective of the present investigation is to computationally study the effect of casing wall motion in an annular turbine rotor impulse cascade with non-uniform inlet flow. To provide non-uniformity at the rotor inlet an annular nozzle cascade is provided at the upstream. The flow in the rotor cascade having 3% tip clearance is analyzed with and without casing wall motion. This value is chosen as it represents most commonly used value in small turbine engines. The casing speed relative to the blade is mass averaged velocity at exit of the rotor cascade. In addition to zero value, three other values, viz. U/C_x=0.5, 1.0 and 1.5 are chosen for the computations. These values represent typical values used in turbine engine practice.

Governing Equations

The governing equations used in the present investigation are presented in the companion paper, Goutham Kumar and Sitaram [6]. The reader is referred to the paper for details.

Methodology

A two-dimensional model of stage (blade profile, camber line, upstream and downstream) created in AUTOCAD 2004 is shown in Fig.1. This drawing is exported to ANSYS ICEM CFD 5.1 and three-dimensional model of annular cascade is created. Unstructured tetrahedral elements are used for meshing. The cascade details are presented in Table-1.

Prismatic elements are used at the boundaries. Meshing is done separately for both rotor and nozzle. The optimized structure of mesh at the mid-span for rotor and nozzle is shown in Fig.2. This mesh is exported to CFX-Pre. The boundary conditions used are shown in Fig.3.

In CFX-Pre, boundary conditions, solver model, convergence criteria are defined and a definition file is created. At the inlet of the nozzle cascade uniform total pressure is applied except in boundary layer region where $1/7^{th}$ power law is used. The nozzle inlet velocity and

Table-1 : Cascade Geometry	
Axial chord, a	92.5 mm
Chord, Ch	95 mm
Hub radius, r_h	200 mm
Casing radius, r_c	300 mm
Blade height, h	100 mm
Spacing, S	52.35 mm (hub) 78.54 (mm (casing)
No. of blades	24
Inlet blade angle, β_1	57.5°
Outlet blade angle, β_2	-62.5°
Incidence, i	0°
Stagger angle, γ	12.5°
Blade camber angle, θ	120°

profiles of flow parameters computed at the rotor blade inlet for zero clearance and zero casing wall motion are presented in the companion paper, Goutham Kumar and Sitaram [6]. The reader is referred to the paper for details. Mass flow rate boundary condition at outlet, periodic boundary condition for periodic surfaces and no slip boundary condition for hub, tip and blade surfaces are applied. No slip condition is used for the case of stationary casing, whereas relative wall condition is used for the case of casing wall motion. Stage interface condition is applied at the rotor-nozzle interface i.e. at the nozzle outlet and rotor inlet. Well known k-ω model is chosen as the turbulence closure. A convergence criterion of 0.00001 is defined.

The definition file is solved in CFX-Solve with PVM local parallel mode. The governing continuity, momentum, energy and turbulence equations are solved until the required convergence criterion is reached. The results file is opened in CFX-Post and results are extracted.

Results and Discussion

The computational results are presented and interpreted in the following sections. Because of large amount of data, only typical data are presented. Casing wall without rotation is referred to as stationary wall case, and casing wall with rotation is referred to as moving wall case in the following sections.

Plots of Streamlines

Streamlines of non-dimensional velocity are drawn for all values of casing speed at two spanwise locations.

Figure 4 shows the streamlines that are released upstream from a spanwise location corresponding to the blade tip. From the figure it is clear that less mass is entrained into the clearance for moving wall cases when compared to stationary wall case. This is due to the obstruction of casing wall boundary layer to the leakage flow, and this obstruction increases with increase in casing wall speed. Hence the amount of mass flow in the clearance region is decreased with increase in casing wall speed.

Figure 4 also shows that in the moving wall cases, most of the leakage flow exiting the clearance on the suction side does not find its way into the leakage vortex. Instead, the exiting leakage flow travels towards the bottom of the passage and joins together with the passage flow. The casing wall boundary layer acts to reduce the amount of clearance available to leakage flow results in reduction in leakage flow boundary layer thickness on the blade tip and a smaller leakage vortex. Fig.4 shows the size of leakage vortex with this expectation.

Velocity Vectors in Blade-to-Blade Plane

Velocity vectors in blade-to-blade plane at different spanwise positions are drawn and discussed for all values of casing wall speed. Velocity vectors in the blade-to-blade plane at η=0.9999 (very close to casing) are shown for all values of casing wall speed in Fig.5. Across the passage, near the pressure surface, the entrainment of fluid into the clearance results in an underturning of the flow for all cases.

In the leading edge region, the entrainment of fluid into the clearance is more apparent in the stationary wall case than in the moving wall cases. This is a direct result of skewed boundary layer on the casing.

Near the leading edge, the flow enters with negligible incidence for stationary wall case where as the tangential component of velocity in casing wall shear layer results in negative incidence for moving wall cases. The velocity on the pressure side is reduced with increase in casing wall speed. This may be due to reduction in leakage flow boundary layer thickness on the blade tip, which is mentioned in the previous section.

Contour Plots

Contour plots of static pressure coefficient in blade-to-blade plane are drawn at the blade tip for all values of casing wall speed. Contour plots of total pressure loss coefficient and non-dimensional velocity at various axial locations in the passage are plotted and analyzed for all values of casing wall speed.

Contour Plots of Static Pressure Coefficient: Fig.6 shows the distribution of static pressure coefficient in blade-to-blade plane at the blade tip for all values of casing wall speed. The pressure coefficient is defined as difference between local static pressure value and inlet midspan static pressure values, non-dimensionalized by inlet midspan dynamic pressure. In the stationary wall case, a low-pressure trough is visible which extends through the entire passage and is situated near to the suction surface. This low pressure region is associated with the leakage vortex. The area of this low pressure region is decreased with increase in casing wall speed. This low pressure region is surrounded by high pressure region in all cases, which indicates that the strength of leakage vortex is diminished locally and the flow is stagnating locally.

The area of this high pressure region is increased with increase in casing wall speed. The unloading of the blade at the pressure side of the clearance is similar for all cases.

Contour Plots of Total Pressure Loss Coefficient: Fig.7 shows contour plots of total pressure loss coefficient at X=0.95. The losses are reduced near the casing wall with increase in casing wall speed. This can be observed by reduction in loss area on the right of the blade pressure surface and very near to the casing. The maximum losses (indicated by red color) on the right of the pressure surface of the blade are also reduced with increase in casing wall speed. Although this sounds good at first, Fig.6 also shows that the motion of the casing wall results in an increase in losses in the negative span direction. This indicates that the casing wall motion decreases the losses in circumferential direction, but increases in spanwise direction.

Contour Plots of Non-dimensional Absolute Velocity: Contour plots of non-dimensional absolute velocity for all values of casing wall speed are drawn at two axial locations. Fig.8 shows contour plots of non-dimensional velocity in the downstream, at X=1.25. The velocity is gained in tangential direction near the casing wall with increase in casing wall speed. Due to the movement of the leakage flow towards the hub by the casing wall motion, the velocity in spanwise direction is reduced with increase in casing wall speed.

Distribution of Static Pressure Coefficient on Blade Surfaces

Figure 9 shows static pressure coefficient distribution on suction and pressure surfaces of the blade at two spanwise locations, η=0.90 and 0.94 for all values of casing wall speed. It has been pointed out in the forgoing text that the casing wall motion affects the pressure distribution on the blade surfaces. At all the spanwise locations, the suction surface pressures are slightly altered, particularly near the trailing edge region, with the casing wall motion, but there is no variation in pressure surface pressures. The pressure on suction surface is reduced with increase in casing wall speed resulting in reduced loading as was also inferred by Yaras and Sjolander [3] as casing wall speed is increased. The distortion of the suction surface pressure field is a consequence of the tip leakage vortex. Thus, the reduced blade loading with increasing wall speed is consistent with the weakening of the tip vortex inferred from the reduced core velocity in gap and observed from the downstream data.

Figure 10 shows the spanwise distribution of lift coefficient for all values of casing wall speed. As the lift coefficient is proportional to area of the blade loading curve, it is also altered with casing wall motion.

Very close to the tip i.e., at η=0.97, the lift coefficient is increased with increase in casing wall speed. It is increased by about 6% for C_c/C_{1xm}=0.5, 19% for C_c/C_{1xm}=1.0 and 44% for C_c/C_{1xm}=1.5 compared to stationary casing. This effect is visible up to η=0.95 and after that the lift coefficient is decreased with increase in the casing wall speed. This is due to the fact that the casing wall motion not only obstructs the penetration of leakage jet into the passage, but it also pushes the leakage fluid into radially inward direction.

Circumferentially Averaged Flow Parameters

The total pressure loss coefficient and flow angle are circumferentially averaged from hub to casing at six different axial locations for all values of casing wall speed; three in the blade passage, X=0.50, 0.75 and 0.95 and three in the downstream X=1.05, 1.25 and 1.50. The values are plotted against the non-dimensional span between hub and casing. Circumferentially averaged flow parameter is defined as follows:

$\bar{q} = \int_0^s q\, c_x\, dy\, dr / \int_0^s c_x\, dy\, r\, dr$, where q is any flow parameter.

Spanwise Variation of Total Pressure Loss Coefficient: Fig.11 shows circumferentially averaged total pressure loss coefficient distribution from hub to casing at six axial locations. At X=0.50, slight decrease in loss coefficient is observed near the casing wall with increase in casing wall speed. But the losses are increased between X=0.95 and X=0.85 with casing wall speed. Similar pattern can be observed at X=0.75 also, where the losses decrease with increase in casing wall speed upto X=0.90, and from thereafter they decrease upto X=0.75. The reduction in losses from the casing wall to certain spanwise location and after that increase in losses with increase in casing wall speed is observed for other axial locations also. This means that the casing wall motion obstructs the penetration of leakage vortex in circumferential direction and pushes radially inwards into the passage. At X=1.50, the effect of tip clearance on the losses can be observed upto η=0.55 (45% of span from casing) for stationary wall case. The extent of the effect is increased to upto η=0.40 (60% of the span from casing) for moving wall cases.

Spanwise Variation of Flow Angle: Spanwise variation of circumferentially averaged flow angle from hub to casing for all values of casing wall speed is shown in Fig.12 at six axial locations. Near the casing wall, decrease in underturning of the flow with increase in casing wall speed can be seen at X=0.50. Similar trend can be observed, near the casing wall at X=0.75 also, but after η=0.90 underturning of fluid increases with casing wall speed. The decrease in underturning of the flow from the casing wall to certain spanwise location, and thereafter increase in underturning is observed at X=0.95, 1.05, 1.25 and 1.50 also. From the figure it is also clear that the casing side passage vortex moves radially inwards with increase in casing wall speed.

Mass Averaged Flow Parameters

Mass averaging of the total pressure loss coefficient and flow angle in different axial planes is done from inlet to outlet of the rotor. These properties are plotted against the non-dimensional axial distance. Mass averaged flow parameter is defined as follows:

$\bar{\bar{q}} = \int_{r_h}^{r_c} \int_0^s q\, c_x\, dy\, dr / \int_h^c \int_0^s c_x\, dy\, r\, dr$, where q is any flow parameter.

Axial Variation of Total Pressure Loss Coefficient from Inlet to Outlet: Axial variation of mass averaged total pressure loss coefficient from inlet to outlet of the rotor cascade is shown in Fig.13 for all values of casing wall speed. From the figure it is clear that, the loss coefficient is slightly increased with increase in casing wall speed. These trends indicate that the relative motion of casing wall has very little effect on total loss field. The casing wall motion reduces the losses in the region near to casing and increases in the region away from the casing. These two effects are roughly equal at all axial stations from inlet to outlet of the cascade, resulting in nearly same magnitudes of losses for all values of casing wall speed.

This should not be construed as identical losses. The flow fields and loss mechanisms are entirely different.

Axial Variation of Flow Angle from Inlet to Outlet: Axial variation of mass averaged flow angle from inlet to outlet of the rotor cascade is shown in Fig.14 for all values of casing wall speed. No variation of flow angle is observed with increase in casing wall speed. The casing wall motion reduces the underturning of the flow in the region near to casing wall and increases in the region away from the casing. So the cumulative effect of these two results in almost identical distributions.

Conclusions

The following conclusions are drawn from the present investigation.

- The casing wall motion and its subsequent shearing on the leakage fluid acts to reduce the leakage flow through the gap, and thus the size of leakage vortex.
- In the stationary wall (casing without rotation) case, almost all of the leakage flow was eventually entrained around the leakage vortex. In moving wall cases, much of the leakage flow traveled around and underneath the leakage vortex, where it developed a strong secondary flow in spanwise direction.
- The casing wall motion reduces the losses in the region near to casing but increases in the region far away from the casing.
- The blade loading and lift coefficient are increased with increase in casing wall motion near the casing and reduced away from the casing.
- Mass averaged total pressure losses in the passage remained very similar in both stationary and moving wall cases.

References

1. Tallman, J. and Lakshminarayana, B., "Numerical Simulation of Tip Leakage Flows in Axial Flow Turbines, with Emphasis on Flow Physics: Part I Effect of Tip Clearance Height", ASME Journal of Turbomachinery, Vol.123, 2001, pp.314-323.

2. Tallman, J. and Lakshminarayana, B., "Numerical Simulation of Tip Leakage Flows in Axial Flow Turbines, with Emphasis on Flow Physics: Part II Effect of Outer Casing Relative Motion", ASME Journal of Turbomachinery, Vol.123, 2001, pp.324-333.

3. Yaras, M. I. and Sjolander, S. A., "Effects of Simulated Rotation on Tip Leakage in a Planar Cascade of Turbine Blades Part I: Gap Flow", ASME Journal of Turbomachinery, Vol.114, 1992, pp.652-659.

4. Yaras, M. I., Sjolander, S. A. and Kind, R. J., "Effects of Simulated Rotation on Tip Leakage in a Planar Cascade of Turbine Blades Part II: Downstream Flow Field", ASME Journal of Turbomachinery, Vol.114, 1992, pp.660-667.

5. Sell, M., Treiber, M., Casciaro, C. and Gyarmathy, G., "Tip-Clearance-Affected Flow Fields in a Turbine Blade Row", Proceedings of Institution of Mechanical Engineers, Part A: Journal of Power and Energy, Vol.213, 1999, pp.309-318.

6. Goutham Kumar, K. and Sitaram, N., "Computational Investigation of Effect of Tip Clearance in an Annular Turbine Rotor Impulse Cascade", Journal of Aerospace Sciences and Technologies, Vol.68, No.4, November 2016, pp.233-244.

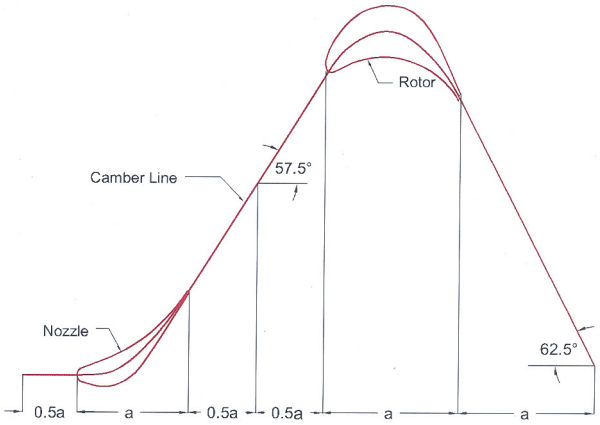

Fig.1 Details of Cascade Geometry

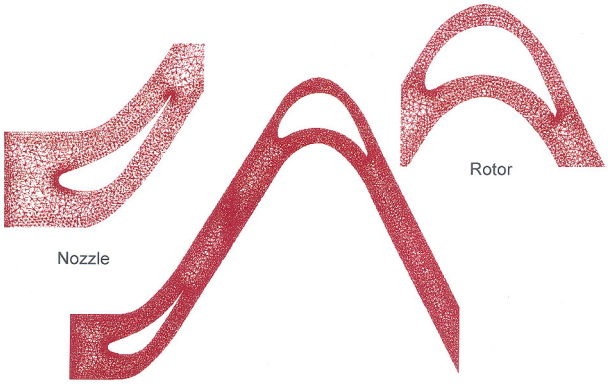

Fig.2 Details of Computational Mesh at Cascade Midspan

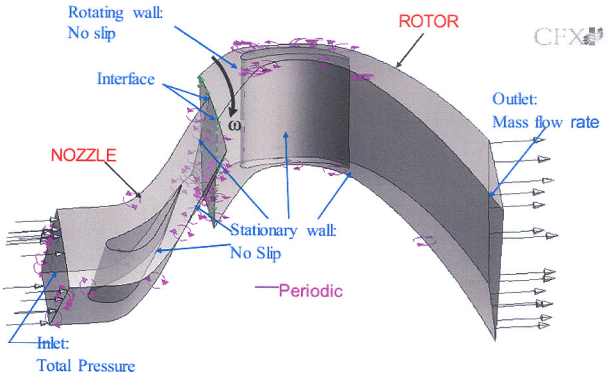

Fig.3 Details of Boundary Conditions with Casing Wall Motion

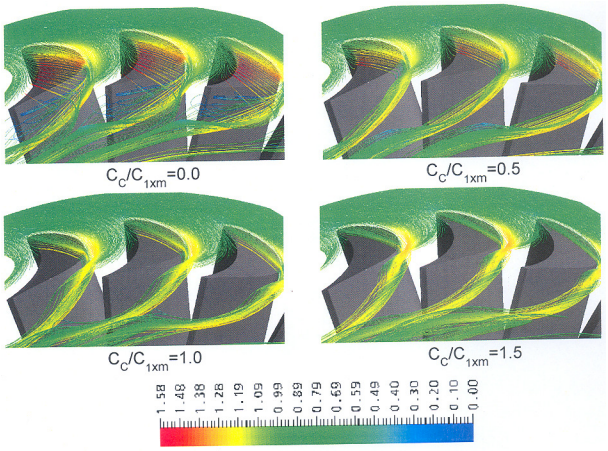

Fig.4 Streamlines of Non-dimensional Velocity at Blade Tip for all Values of Casing Wall Speeds

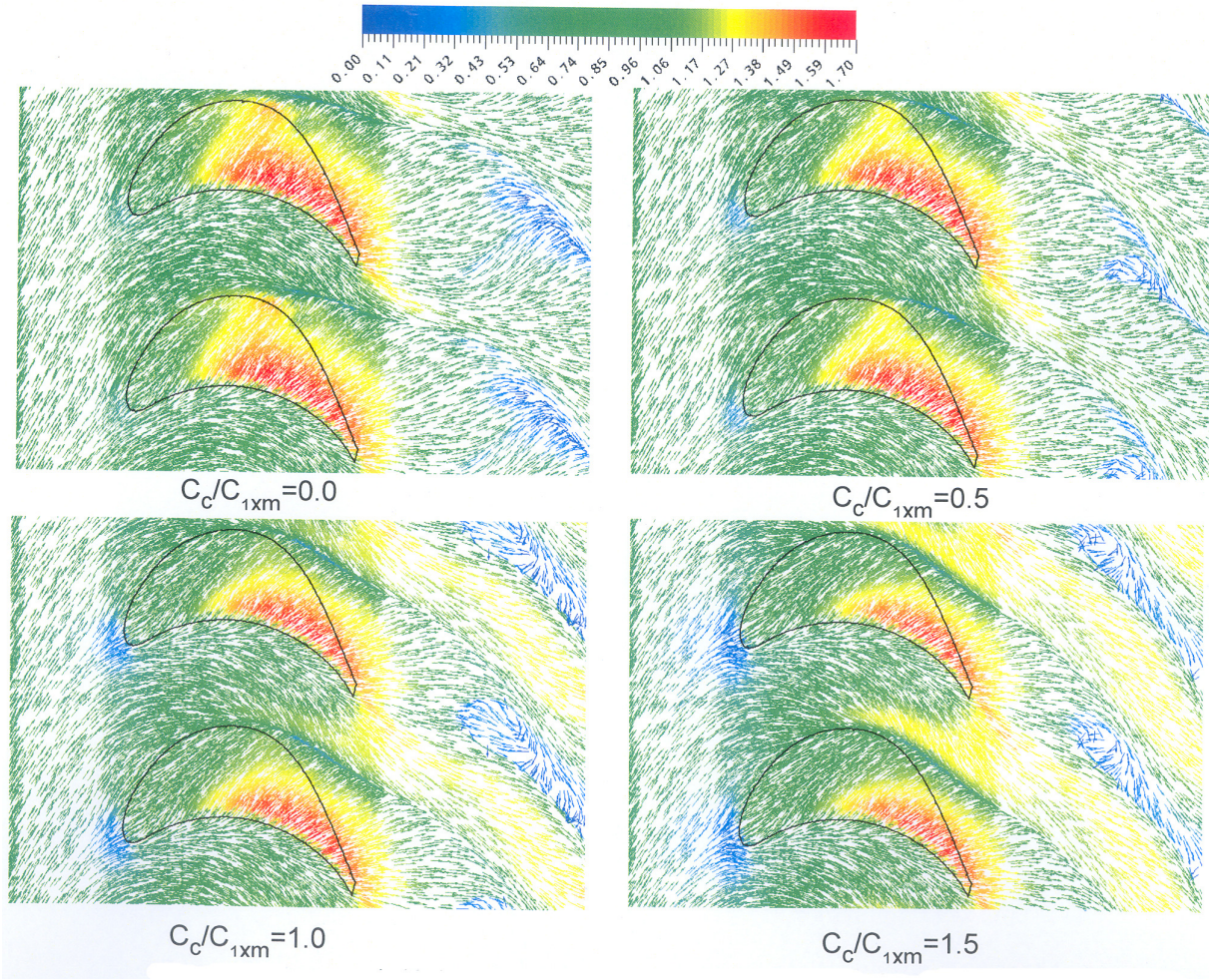

Fig.5 Velocity Vectors in Blade-to-Blade Plane at η=0.9999 for all Values of Casing Wall Speed

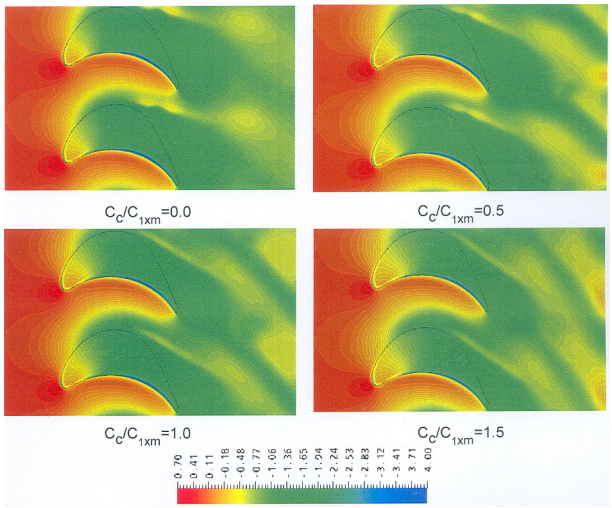

Fig.6 Contour Plots of Static Pressure Coefficient at Tip for all Values of Casing Wall Speed

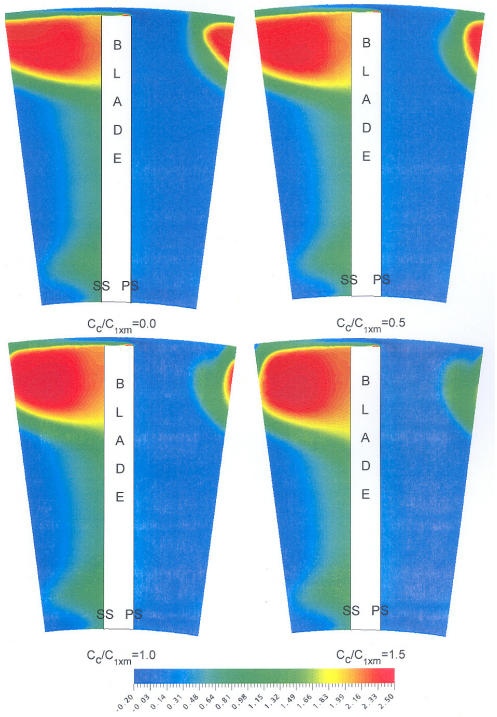

Fig.7 Contour Plots of Total Pressure Loss Coefficient at X=0.95 for all Values of Casing Wall Speed

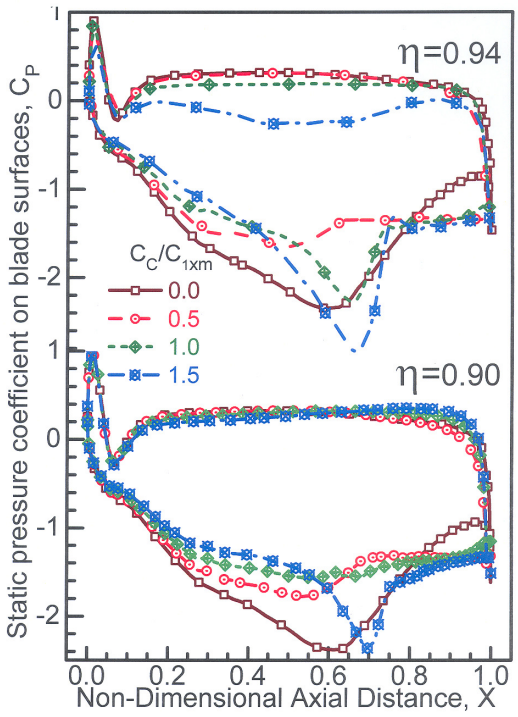

Fig.9 Distribution of Static Pressure Coefficient on Blade Surfaces at η=0.94 and 0.90 for all Values of Casing Wall Speed

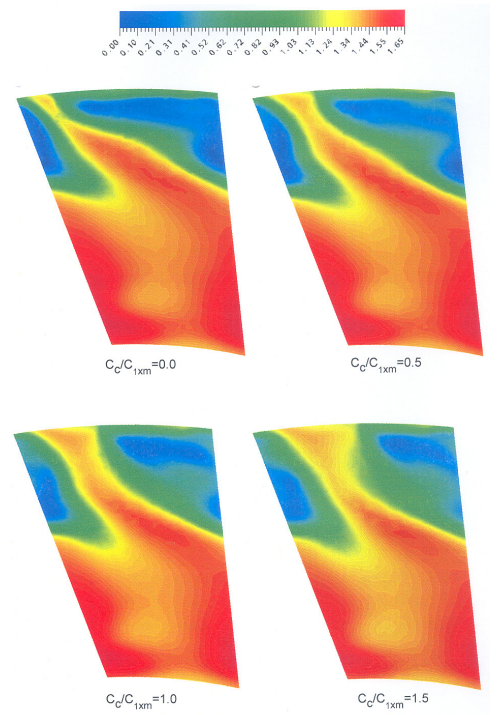

Fig.8 Contour Plots for Non-dimensional Velocity at X=1.25 for all Values of Casing Wall Speed

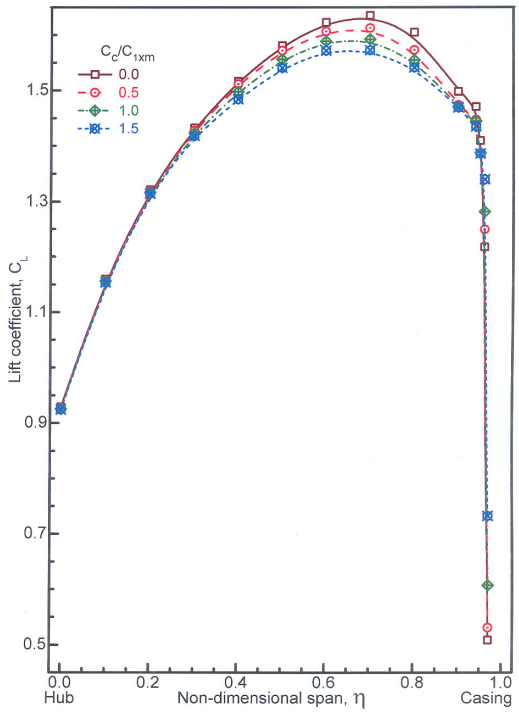

Fig.10 Spanwise Variation of Lift Coefficient for all Values of Casing Wall Speed

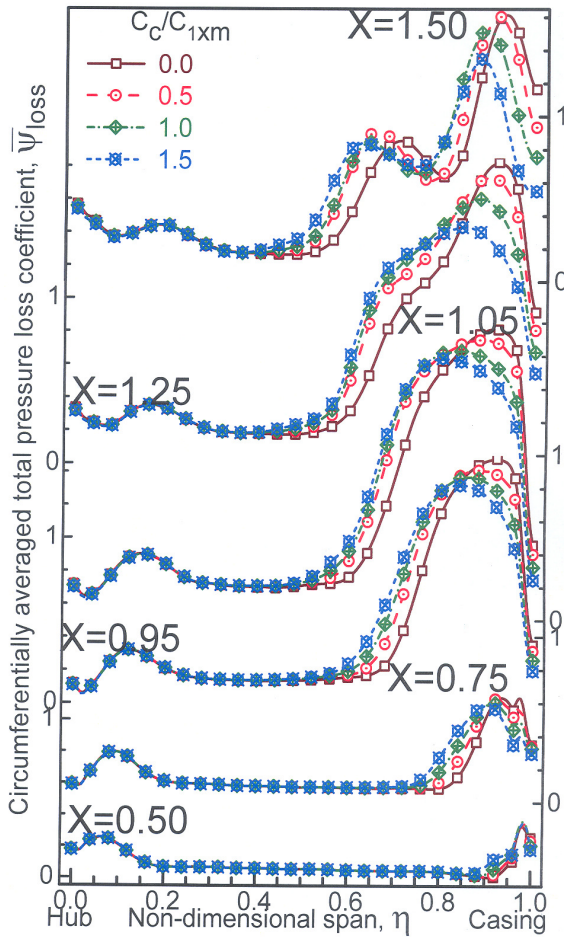

Fig.11 Spanwise Variation of Circumferentially Averaged Total Pressure Loss Coefficient for all Values of Casing Wall Speed

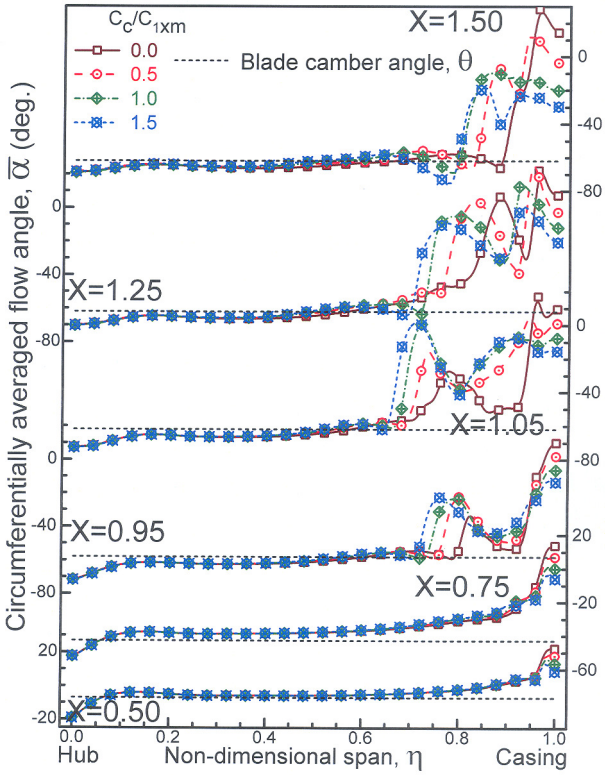

Fig.12 Spanwise Variation of Circumferentially Averaged Flow Angle for all Values of Casing Wall Speed

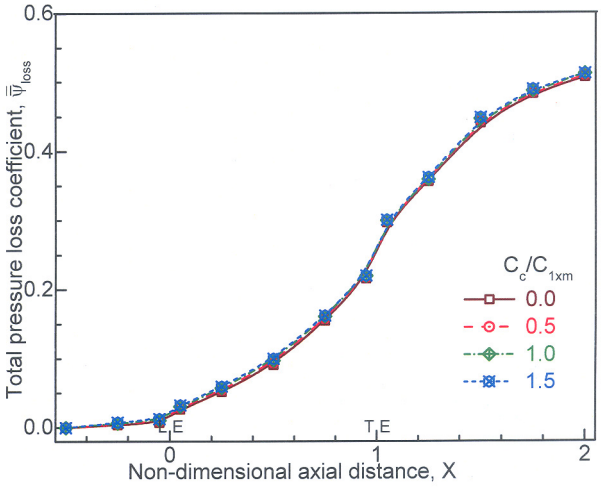

Fig.13 Axial Variation of Mass Averaged Total Pressure Loss Coefficient for all Values of Casing Wall Speed

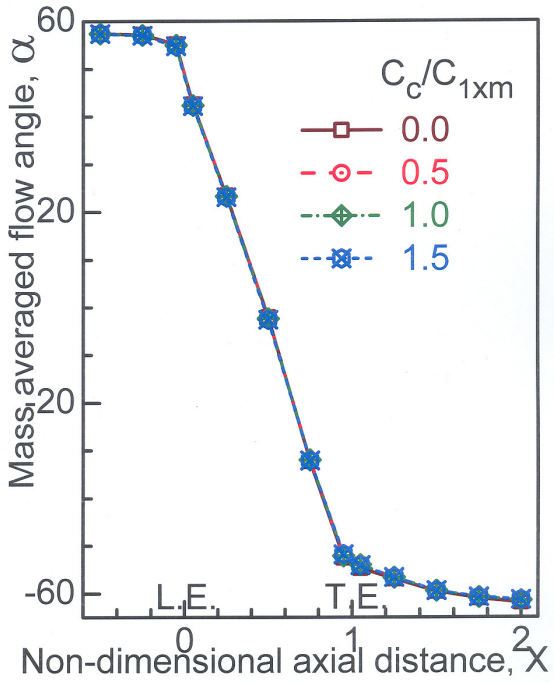

Fig.14 Axial Variation of Mass Averaged Flow Angle for all Values of Casing Wall Speed